Type-1 Fuzzy Logic System Applied to Classification of Rail Head Defects

Eduardo Aguiar[1], Lucas Silva[1], Adler Moreira[1], Leonardo Fonseca[1], Fernando Nogueira[1], Marley Vellasco[2], and Moises Ribeiro[1]

[1] Federal University of Juiz de Fora, Juiz de Fora/MG, Brazil
{eduardo.aguiar,lucas.verneck,adler.ferreira,fernando,mribeiro}@
engenharia.ufjf.br, leonardo.goliatt@ufjf.edu.br
[2] Pontifical Catholic University of Rio de Janeiro, Rio de Janeiro/RJ, Brazil
marley@ele.puc-rio.br

Abstract. This paper focuses on the classification of rail head defects, through images acquired by a rail inspection vehicle. With this regards, we discuss the use of a type-1 and singleton/non-singleton fuzzy logic system to dealing with this problem, based on a numerical data set composed of images provided by a Brazilian railway company, which covers the four possible rail head defects (cracking, flaking, head check and spalling). We use geometric correction through a two-dimensional affine transformation and a gray level co-occurrence matrix to extract the features to be used as an input of the classifiers. Finally, we present performance analysis in terms of classification ratio and convergence speed. The reported results show that the chosen non-singleton model result in improved efficiency and it can be used to handle uncertainties associated with this kind of problem.

Keywords: fuzzy logic systems, image processing, rail head, classification, defects.

1 Introduction

Railways are a network of distributed rails which aims to connecting cities, states and countries. In most cases, they have been used for heavy loads, what impacts directly on rails, increasing its defects through material fatigue. Researches have been made to solve relevant questions in railways. As consequence, there is a increasing interest in transportation researchers to exploiting the feasibility of applying image processing and computational intelligence paradigms to address critical problems in order to improve the efficiency, safety, and environmental compatibility of transportation systems. Some problems, as detection of surface defects on rails, have been widely approached.

An intelligent vision detection system for discrete surface defects and focuses on image enhancement and automatic thresholding was discussed in [1]. Moreover, [2] proposed an automatic method for detecting one specific type of railway surface defect called squats using axle box acceleration measurements

on trains. The authors in [3] presented and validated a fuzzy diagnosis method based on image processing, basing in an evaluation and integration between images obtained from camera and depth data measured with laser meter. In [4] is discussed an inspection method for rail surface defects based on automated machine vision system, analyzing two kinds of defect images including spalling of rail head and cracks in surface. In addition, [5] addresses the heavy rail surface defect detection according to their characteristics, uneven brightness and noise, and uses mathematical morphology of multi-scale and dual-structure elements as detection bases. In [6], the authors presented a new vision based on inspection technique for detecting special rolling contact fatigue defects that particularly occur on rail head surface, implementing an automatic detection system.

Among all possible defects that can occur in a rail head, the four main ones are cracking [7], flaking [8], head check and spalling [9]. A common aspect of all previous works (see references [1]-[6]) is the focus on the detection of the existence of a defect, and not on classify different types of defects, such as those contemplated in this work. This work focuses on classify types of rail head surface defects that are commonly studied due to its severity and occurrence: cracking, flaking, head check and spalling. It is important to emphasize that the classification of these specific types of defects and the normal condition by extracting textures of rail head pictures is novel.

The main contributions of this work are summarized as follows:

- We approach four types of defects that can occur in a rail head surface. The combined study of cracking, flaking head-check and spalling linked to rail head surface has never been addressed before.
- We use geometric correction through a two-dimensional affine transformation [10] to facilitate the image processing and a gray level co-occurrence matrix (GLCM)to analyse textures on images [11, 12].
- We present performance analysis in terms of convergence speed, classification ratio and efficiency by using a data set constituted by images acquired from a rail inspection vehicle. Additionally, we show a comparative analysis among the proposed models based on type-1 and singleton/non-singleton FLS techniques trained by steepest descent method.

Our major conclusions are as follows:

- The two-dimensional affine transformation geometric correction and feature extraction through GLCM is effective for the current application.
- The classification ratio yielded by the non-singleton model are higher than those obtained with the singleton when a higher degree of uncetainties is presented in the input data.

The rest of the paper is organized as follows: Section 2 deals with the problem formulation. Section 3 discusses the results of computer simulations. Section 4 states the main conclusions regarding the proposals.

2 Problem Formulation

Among all possible defects that can occur on the rail head, the four main ones are cracking, flaking, head check and spalling. Let $\mathbf{A} \in \mathbb{R}^{n \times m}$ be a matrix constituted by elements of an image of the rail head. Figure 1 shows the paradigm used for the classification of events. In the block "Geometric Correction", $\mathbf{P}$ refers to cracking, flaking, head check, spalling and normal condition of the rail head. The block "Feature Extraction" provides extracted features $\mathbf{K}_{p_c}$, $\mathbf{K}_{p_f}$, $\mathbf{K}_{p_h}$, $\mathbf{K}_{p_s}$ and $\mathbf{K}_{p_n}$ vectors from $\mathbf{P}$. The block "Classification" applies one of the classification techniques discussed in this work to obtain the output vector $\mathbf{S}$, thereby identifying the type of defect. We use five independent classifiers, one for each possible event.
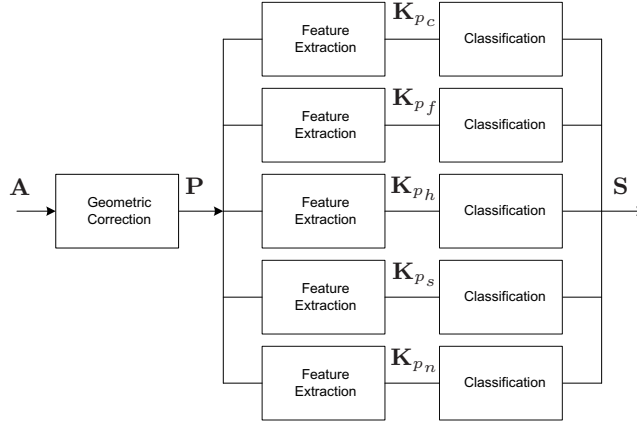

Fig. 1. Block diagram of the scheme for classification of events.

The classification of events in the matrix $\mathbf{A}$ can be formulated as a simple decision between hypotheses related to the occurrence of the events covered in this work, as shown below:

$$
\begin{aligned}
\mathcal{H}_{A,0} &: \mathbf{A} = \mathbf{A}_{crack}, \\
\mathcal{H}_{A,1} &: \mathbf{A} = \mathbf{A}_{flak}, \\
\mathcal{H}_{A,2} &: \mathbf{A} = \mathbf{A}_{head}, \\
\mathcal{H}_{A,3} &: \mathbf{A} = \mathbf{A}_{spall}, \\
\mathcal{H}_{A,4} &: \mathbf{A} = \mathbf{A}_{norm}.
\end{aligned}
\tag{1}
$$

In which $\mathbf{A}_{crack}$, $\mathbf{A}_{flak}$, $\mathbf{A}_{head}$, $\mathbf{A}_{spall}$ and $\mathbf{A}_{norm}$ denotes the cracking, flaking, head check, spalling and normal condition of the rail head, respectively.

The proposed model makes it possible to reduce the impact on trains operation and on preventive maintenance, since the interventions are performed at

specific sites where the defect was detected. The model responsible for classifying the type of defect shall assist to:

- eliminate visual inspection of the rails and images acquired by the equipment;
- reduce the number of unproductive hours in maintenance, due to the knowledge of defects before moving the maintenance team to the field;
- reduce the number of recurrent preventive interventions;
- increase productivity of rail operations, given the reduction in time of operational maintenance.

The classifiers used are based on type-1 and singleton fuzzy logic system (FLS) [13, 14] and type-1 and non-singleton FLS. Next section develops the latter FLS.

2.1 Geometric Correction

The geometric correction through a two-dimensional affine transformation [10] aims to facilitate the image processing becoming the original image parallel to Y axis of the cartesian coordinate system. The affine transformation consists of a linear transformation followed by a translation. This transformation preserves the parallelism property. If two lines are parallel before the transformation, these lines are also parallel after processing.

2.2 Texture Feature Extraction Based On Gray Level Co-Occurrence Matrix

The gray level co-occurrence matrix (GLCM) has been one of the most used methods to analyze textures on images [11,12] and it is a two-dimensional dependence matrix that considers the spatial relationship between neighboring pixels. The GLCM describes the textures of the images based on the frequency in which two gray levels separated by a distance d in a θ direction occur in the image. The texture information of an image can be described by GLCM functions, as shown below

$$
G = \begin{bmatrix} p(1,1) & p(1,2) & \cdots & p(1,n) \\ p(2,1) & p(2,2) & \cdots & p(2,n) \\ \vdots & \vdots & \ddots & \vdots \\ p(n,1) & p(n,2) & \cdots & p(n,n) \end{bmatrix},
\tag{2}
$$

where and $p(i,j)$ denotes the value of the matrix element having index (i,j) and n is the number of gray levels present in the image. For the construction of a GLCM, we must define the spatial relationship composed by the distance d, in pixel unit, and the adopted direction from the reference pixel, denoted by θ. Figure 2 shows us the possible angles to be adopted from the reference pixel.
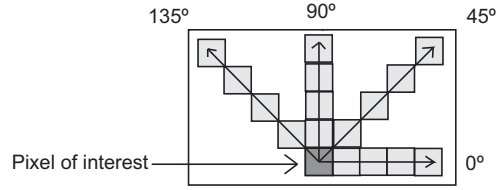
Fig. 2. In addition to $\theta = 0°$, we can choose other three values to the reference angle. Thus, the GLCM provided from Figure 2 has $\theta = \{0°, 45°, 90°, 135°\}$ and $d = 4$.
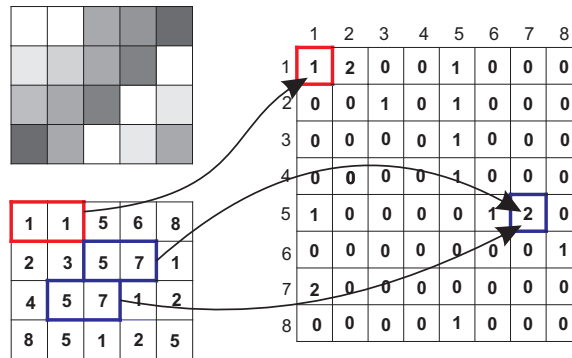

Fig. 3. An example of GLCM construction from a small image, where $d = 1$, $\theta = 0°$ and the gray levels range from 1 to 8.

Figure 3 show us how is calculated an GLCM for $d = 1$ and $\theta = 0°$. The element $p(1,1)$ contains the value 1 because there is only one instance in the input image where two horizontally adjacent pixels have the values 1 and 1, respectively. The element $p(5,7)$ contains the value 2 it has two instances where two horizontally adjacent pixels have the values 5 and 7. Thus, each element $p(i,j)$ of the grey level co-occurrence matrix represents the instances there has been a transition from gray level i to j considering the distance d between the two neighboring pixels in the direction θ. The GLCM can be normalized by dividing each entry by the number of neighboring resolution cell pairs. Each value is the probability of a transition between gray levels under specified conditions of distance and direction. Based on the co-occurrence matrices, the equations $(3)-(6)$ describing the energy (ASM), contrast (CON), correlation (COR) and homogeneity (HOM), that aims to represent characteristic textures. Note that μ_i, μ_j, σ_i and σ_j are the mean and standard deviation, respectively [11].

$$ASM(i,j) = \sum_{i=1}^{n} \sum_{j=1}^{n} p(i,j)^2, \tag{3}$$

$$CON(i,j) = \sum_{i=1}^{n}\sum_{j=1}^{n}(i-j)^2 p(i,j), \qquad (4)$$

$$COR(i,j) = \sum_{i=1}^{n}\sum_{j=1}^{n}\frac{(i-\mu_i)(j-\mu_j)}{\sigma_i \sigma_j}p(i,j), \qquad (5)$$

$$HOM(i,j) = \sum_{i=1}^{n}\sum_{j=1}^{n}\frac{p(i,j)}{1+|i-j|}. \qquad (6)$$

2.3 Type-1 and Singleton Fuzzy Logic System

Considering singleton fuzzification, max-product composition, product implication and height defuzzifier and leaving open the choice of membership function, it is simple to show that the output of a type-1 and singleton FLS is [14]:

$$f_s(\mathbf{x}) = \sum_{l=1}^{M}\theta_l \phi_l(\mathbf{x}), \qquad (7)$$

where $\phi_l(\mathbf{x})$ is called fuzzy basis function (FBF) [14], that is given by:

$$\phi_l(\mathbf{x}) = \frac{\prod_{k=1}^{p}\mu_{F_k^l}(x_k)}{\sum_{l=1}^{M}\prod_{k=1}^{p}\mu_{F_k^l}(x_k)}$$

$$= \frac{\prod_{k=1}^{p}\exp\left(-\frac{\left(x_k^{(q)}-m_{F_k^l}\right)^2}{2\sigma_{F_k^l}^2}\right)}{\sum_{l=1}^{M}\left[\prod_{k=1}^{p}\exp\left(-\frac{\left(x_k^{(q)}-m_{F_k^l}\right)^2}{2\sigma_{F_k^l}^2}\right)\right]}, \qquad (8)$$

Given a set of input-output pairs $(\mathbf{x}^{(q)} : y^{(q)})$, where q denotes the qth iteration and each iteration consists of the presentation of all samples, the problem consists, in fact, of minimizing the following cost function [14]:

$$J(\mathbf{w}^{(q)}) = \frac{1}{2}\left[f_s(\mathbf{x}^{(q)}) - y^{(q)}\right]^2. \qquad (9)$$

The result is

$$m_{F_k^l}(q+1) = m_{F_k^l}(q) - \alpha\left[f_s(\mathbf{x}^{(q)}) - y^{(q)}\right] \times$$
$$\left[\theta_l(q) - f_s(\mathbf{x}^{(q)})\right]\frac{\left[x_k^{(q)}-m_{F_k^l}(q)\right]}{\sigma_{F_k^l}^2(q)}\phi_l(\mathbf{x}^{(q)}) \qquad (10)$$

$$\theta_l(q+1) = \theta_l(q) - \alpha\left[f_s(\mathbf{x}^{(q)}) - y^{(q)}\right]\phi_l(\mathbf{x}^{(q)}) \qquad (11)$$

and

$$\sigma_{F_k^l}(q+1) = \sigma_{F_k^l}(q) - \alpha \left[f_s(\mathbf{x}^{(q)}) - y^{(q)} \right] \times$$
$$\left[\theta_l(q) - f_s(\mathbf{x}^{(q)}) \right] \frac{\left[x_k^{(q)} - m_{F_k^l}(q) \right]^2}{\sigma_{F_k^l}^3(q)} \phi_l(\mathbf{x}^{(q)}) \qquad (12)$$

Note that $\alpha \in \mathbb{R} | 0 \leq \alpha < 1$ is the step size used to update parameters from type-1 and singleton FLS.

2.4 Type-1 and Non-Singleton Fuzzy Logic System

Considering non-singleton fuzzification, max-product composition, product implication and height defuzzifier and gaussian membership functions, the output of a type-1 and non-singleton FLS is [14]

$$f_{ns}(\mathbf{x}) = \sum_{l=1}^{M} \theta_l \phi_l(\mathbf{x}), \qquad (13)$$

where $\phi_l(\mathbf{x})$ is called fuzzy basis function (FBF) [14] and is given by

$$\phi_l(\mathbf{x}) = \frac{\prod_{k=1}^{p} \exp\left(-\frac{1}{2} \frac{\left(x_k^{(q)} - m_{F_k^l} \right)^2}{\sigma_{F_k^l}^2 + \sigma_X^2} \right)}{\sum_{l=1}^{M} \left[\prod_{k=1}^{p} \exp\left(-\frac{1}{2} \frac{\left(x_k^{(q)} - m_{F_k^l} \right)^2}{\sigma_{F_k^l}^2 + \sigma_X^2} \right) \right]}, \qquad (14)$$

where $\mathbf{x} \in \mathbb{R}^{K_p}$ is the vector constituted by K_p elements, $\prod$ denotes the product operator, $m_{F_k^l}$ and $\sigma_{F_k^l}$ are the mean and variance associated to the k-th input feature of the l-th rule. θ_l is the weight associated with the l-th rule, $l = 1, \ldots, M$. σ_X is the variance associated to each input membership function. The subscript "ns" in $f_{ns}(\mathbf{x})$ informs that this is a non-singleton FLS. The equations for training type-1 and non-singleton differ from those applied to type-1 and singleton due to the presence of σ_X.

Consider a set of input-output pairs $(\mathbf{x}^{(q)} : y^{(q)})$, where q denotes the qth iteration. To obtain the suitable parameters of $f_{ns}(\mathbf{x})$ for our classification problem, the task is to minimize the following cost function [14]

$$J(\mathbf{w}^{(q)}) = \frac{1}{2} \left[f_{ns}(\mathbf{x}^{(q)}) - y^{(q)} \right]^2. \qquad (15)$$

By applying steepest descent method, we obtain

$$m_{F_k^l}(q+1) = m_{F_k^l}(q) - \alpha \left[f_{ns}(\mathbf{x}^{(q)}) - y^{(i)} \right] \times$$
$$\left[\theta_l(q) - f_{ns}(\mathbf{x}^{(q)}) \right] \left[\frac{x_k^{(q)} - m_{F_k^l}(q)}{\sigma_X^2(q) + \sigma_{F_k^l}^2(q)} \right] \phi_l(\mathbf{x}^{(q)}), \qquad (16)$$

$$\theta_l(q+1) = \theta_l(q) - \alpha \left[f_{ns}(\mathbf{x}^{(q)}) - y^{(q)} \right] \phi_l(\mathbf{x}^{(q)}), \tag{17}$$

$$\sigma_{F_k^l}(q+1) = \sigma_{F_k^l}(q) - \alpha \left[f_{ns}(\mathbf{x}^{(q)}) - y^{(q)} \right] \times$$
$$\left[\theta_l(q) - f_{ns}(\mathbf{x}^{(q)}) \right] \sigma_{F_i^l}(q) \left[\frac{x_k^{(q)} - m_{F_k^l}(q)}{\sigma_X^2(q) + \sigma_{F_k^l}^2(i)} \right]^2 \phi_l(\mathbf{x}^{(q)}), \tag{18}$$

and

$$\sigma_X(q+1) = \sigma_X(q) - \alpha \left[f_{ns}(\mathbf{x}^{(q)}) - y^{(q)} \right] \times$$
$$\left[\theta_l(q) - f_{ns}(\mathbf{x}^{(q)}) \right] \sigma_X(q) \left[\frac{x_k^{(q)} - m_{F_k^l}(q)}{\sigma_X^2(q) + \sigma_{F_k^l}^2(q)} \right]^2 \phi_l(\mathbf{x}^{(q)}). \tag{19}$$

3 Experimental Results

Performance analyses discussed in this section made use of measured data set provided by MRS Logística (`https://www.mrs.com.br/`). The data set consists of images captured by a camera attached to a special car service that runs the permanent way. The images of the rail head are taken in the order of three images per meter.

The acquired images fall within the following five classes: cracking, flaking, head check, spalling and normal condition of the rail head. As a result, there are 88 images for each of the five classes. We show samples of such images in Figure 4.
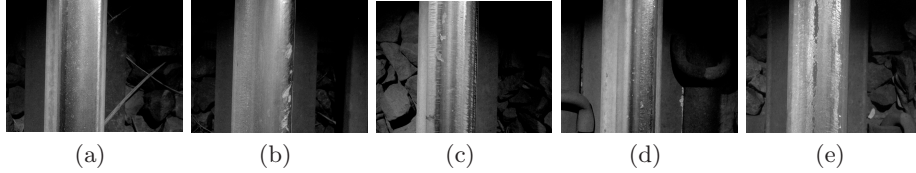

(a)	(b)	(c)	(d)	(e)

Fig. 4. Typical samples for the five classes. a) Normal condition. b) Cracking. c) Flaking. d) Head check. e) Spalling.

Each type-1 and singleton/non-singleton FLS is composed of four rules (M = 4), two rules for the class that has the presence of the event and another two for the class that does not have the presence of the event. The adopted step size for type-1 and singleton/non-singleton FLS trained with the steepest descent method is $\alpha = 0.0001$. The performance gains in term of accuracy and convergence speed are not relevant when $M \neq 4$ or $\alpha \neq 0.0001$. We have initialized the parameters of membership functions heuristically from the calculation of means and variances of the features vector constituted by the elements extracted from

the GLCM. Furthermore, we equally and randomly distributed the data set in training and test sets and considered 100 epochs for the training phase.

Following the block diagram of the classification technique depicted in Figure 1, we adopted techniques for geometric correction through affine transformation and feature extraction using GLCM. After evaluating the performance with different features extracted from GLCM, we chose $\theta = \{0°, 45°, 90°, 135°\}$, $d = 100$ and use the obtained features as input of the proposed classifiers. For comparison purpose, we implemented the type-1 and singleton/non-singleton FLS [13,14] in order to classify defects in a rail head. Observing the block diagram in Figure 1, that $y^{(q)} = 1$ means that the matrix $\mathbf{A}$, constituted by pixels of taken image of the rail head is associated with the occurrence of the defect. On the other hand, $y^{(q)} = -1$ states that the matrix $\mathbf{A}$ is associated with the absence of defect.

3.1 Convergence Speed Analysis

Figure 5 shows the convergence speed for the normal condition, cracking, flaking, head check and spalling classes.

Expressly it can be seen that the singleton model had a higher convergence speed for the classification of normal condition and cracking events. For flaking defect both classifiers had a pretty similar speed convergence, in contrast, for head check and spalling classes the non-singleton FLS had a better performance in this regard.

Looking for the spalling defect it can be noted a great difference between the two curves, the singleton FLS presented a low performance in relation to the non-singleton FLS for the event classification. This difference was due to a higher degree of uncertainties associated with the measured data regarding to this class. Thus the non-singleton model assumed a considerably higher performance when data with associated uncertainties were presented to the classifiers.
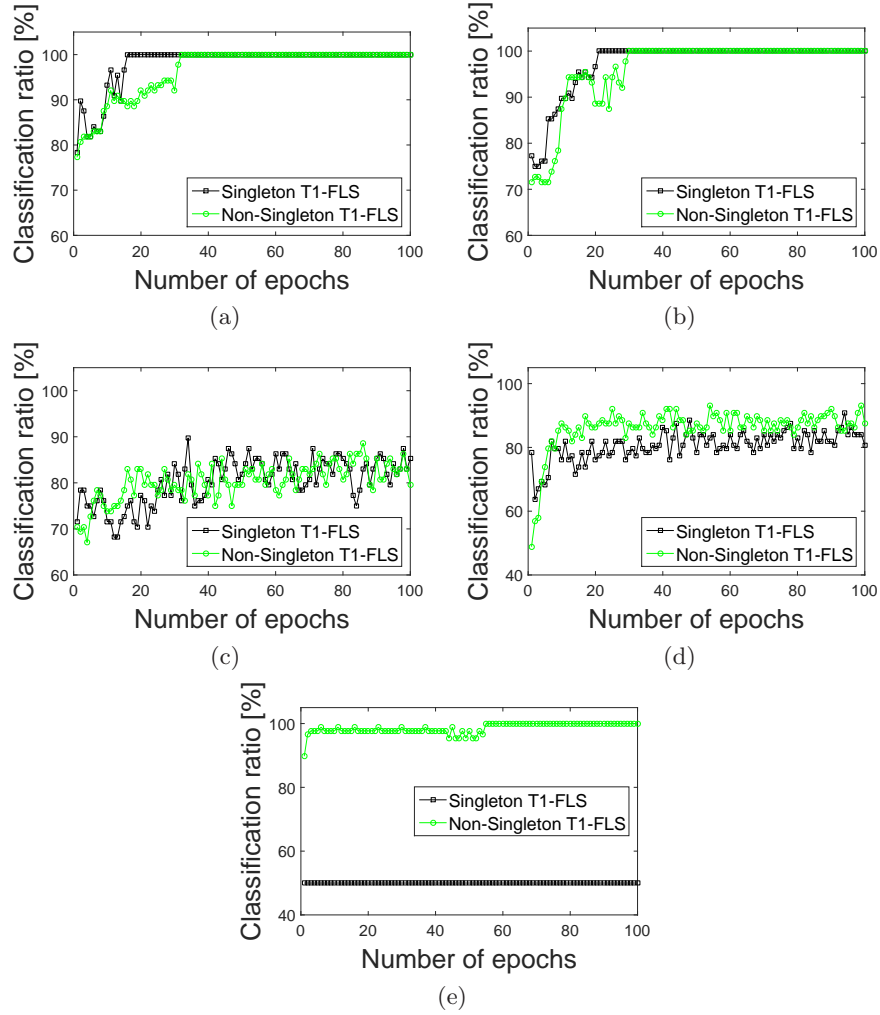
Fig. 5. Convergency speed for a) Normal Condition, b) Cracking, c) Flaking, d) Head Check and e) Spalling.

3.2 Classification Rate Analysis

The numerical results presented in Table 1 indicates the correct classification rates in terms of percentage for the type-1 and singleton/non-singleton FLS, both the training phase and for the test phase. The efficiency ρ is the arithmetic mean of the best achieved performances considering each event. We see that the non-singleton model in addition to having a reasonable speed of convergence, they provide higher efficiency when compared with the type-1 and singleton FLS.

According to the results, the type-1 and singleton FLS had a similar classification rate for the normal condition and cracking events when compared with type-1 and non-singleton FLS, with 100.0% of rate for both. Still analyzing Table 1, we can note that the singleton model has a lower efficiency due to its low rating fee to the spalling event caused by lack of performance when working with data that present uncertainties.

Table 1. Classification Rate.

Events	Singleton FLS		Non-Singleton FLS	
	Training	Test	Training	Test
Normal Condition	100.0	100.0	100.0	100.0
Cracking	100.0	100.0	100.0	100.0
Flaking	85.2	85.2	79.6	79.6
Head Check	80.7	80.7	87.5	87.5
Spalling	50.0	50.0	100.0	100.0
Efficiency (ρ)	**83.2**	**83.2**	**93.4**	**93.4**

4   Conclusions

In this work we discussed the use of image processing and computational intelligence techniques, introducing the use of the type-1 and singleton/non-singleton concept aiming to analyze theirs effectiveness to classify typical rail head defects. The geometric correction through a two-dimensional affine transformation and the extraction of GLCM-based features have proved to be relevant and have contributed to consistency and a reduction in the dimensionality of the data to be presented to the classifiers.

Considering a reduced number of epochs, the numerical results obtained through the use of measured data set showed that both models discussed have similar and relevant convergence speed. Additionally, the type-1 non-singleton FLS model reached a higher classification rates than those obtained with the type-1 singleton FLS, specially when there are uncertainties in the input data and the number of epochs in the training phase is limited.

In all analyzed situations the non-singleton model turn out to be an attractive option due to their high classification rate and efficiency reaching percentages in the order of 93.4%. Additionally, it is notorious that non-singleton FLS handled satisfactorily the presence of uncertainties in the measured data showing better classification rates than singleton FLS, thus proving in fact be a attractive choice for the rail head defect classification problem.

Future work is to prototype an equipment to be integrated into the existing rail head supervision system in the company MRS Logística S.A. We intend to improve the preprocessing of images, through the research of segmentation tools and other techniques for feature extraction, in order to get a better performance. Also, we plan to investigate the usefulness of non-singleton type-1 FLS to handle the presence of uncertainty in the measured data set.

References

1. Li, Q., Ren, S.: A visual detection system for rail surface defects. IEEE Transactions on Systems, Man, and Cybernetics **42**(6) (Nov. 2012) 1531–1542
2. Molodova, M., Li, Z., Nunez, A., Dollevoet, R.: Automatic detection of squats in railway infrastructure. IEEE Transactions on Intelligent Transportation Systems **15**(5) (Oct. 2014) 1980–1990
3. Karaduman, G., Karakose, M., Akin, E.: Experimental fuzzy diagnosis algorithm based on image processing for rail profile measurement. *in* Proc. International Symposium Mechatronika (Dec. 2012) 1–6
4. Liu, Z., Wang, W., Zhang, X., Jia, W.: Inspection of rail surface defects based on image processing. *in* Proc. International Asia Conference on Informatics in Control, Automation and Robotics **1** (Mar. 2010) 472–475
5. Hu, G., Xiong, L., Tang, J.: Heavy rail surface defects detection based on the morphology of multi-scale and dual-structure elements. *in* Proc. Chinese Automation Congress (Nov. 2015) 2126–2129
6. Jie, L., Siwei, L., Qingyong, L., Hanqing, Z., Shengwei, R.: Real-time rail head surface defect detection: A geometrical approach. *in* Proc. IEEE International Symposium on Industrial Electronics (Jul. 2009) 769–774
7. Zhang, H.Y., Feng, D., cong Yao, J., ling Yu, Y.: Guided wave propagation characteristics in the rail with a crack defect. *in* Proc. Symposium on Piezoelectricity, Acoustic Waves and Device Applications (Oct. 2013) 1–4
8. Chang, H., Wilson, C., Jackson, J.: Eliminating polymer flake defects using an oxygen free chemistry. *in* Proc. IEEE International Symposium on Semiconductor Manufacturing Conference Proceedings (Oct. 1997) 91–93
9. Stone, D., Carlson, F., Bachhuber, C.: Effect of brake-system components on wheel spalling. *in* Proc. IEEE Joint Railroad Conference (Apr. 1999) 177–183
10. Lin, H., Du, P., Zhao, W., Zhang, L., Sun, H.: Image registration based on corner detection and affine transformation. *in* Proc. 3rd International Congress on Image and Signal Processing (Oct. 2010) 2184–2188
11. Haralick, R., Shanmugam, K., Dinstein, I.: Textural features for image classification. IEEE Transactions on Systems, Man and Cybernetics **3**(6) (Nov. 1973) 610–621
12. Yang, J., Guo, J.: Image texture feature extraction method based on regional average binary gray level difference co-occurrence matrix. *in* Proc. International Conference on Virtual Reality and Visualization (Nov. 2011) 239–242
13. de Aguiar, E.P., Nogueira, F.M.A., Amaral, R.P., Fabri, D.F., Rossignoli, S.C., Ferreira, J.G., Vellasco, M.M.B.R., Tanscheit, R., Vellasco, P.C.S., Ribeiro, M.V.: Eann 2014: a fuzzy logic system trained by conjugate gradient methods for fault classification in a switch machine. Neural Computing and Applications (2015) 1–15
14. Mendel, J.M.: Uncertain Rule-Based Fuzzy Logic Systems: Introduction and New Directions. Prentice Hall PTR (2001)